A first comparison between ionospheric and surface level magnetic fields at Mars

Matthew O Fillingim[1], Catherine L. Johnson[2], Anna Magdalena Mittelholz[3], Benoit Langlais[4], Christopher T. Russell[5], Steven P. Peter Joy[5], Peter J Chi[5], Robert James Lillis[1], Jared Randolph Espley[6], Suzanne E. Smrekar[7], William Bruce Banerdt[8], and Bruce M. Jakosky[9]

[1]University of California, Berkeley
[2]University of British Columbia
[3]The University of British Columbia
[4]Laboratoire de Planétologie et Géodynamique, Univ. Nantes, Univ. Angers, CNRS, UMR 6112
[5]University of California Los Angeles
[6]NASA Goddard
[7]Jet Propulsion Laboratory
[8]Jet Propulsion Lab (NASA)
[9]University of Colorado Boulder

November 21, 2022

Abstract

With both the Mars Atmosphere and Volatile Evolution (MAVEN) mission and the Interior Exploration using Seismic Investigations, Geodesy and Heat Transport (InSight) mission concurrently operating at Mars, we are able to make two point comparisons of the vector magnetic field at Mars for the first time. During MAVEN overflights of the InSight landing site, we compared deviations in the ionospheric magnetic field to variations in the surface level magnetic field. We find significant orbit to orbit variability in the magnitude and direction of the ionospheric magnetic field as well as significant day to day variability of the surface level magnetic field. We attribute this variability to time varying ionospheric currents. However, when analyzing the ensemble of 16 individual MAVEN overflights of the InSight landing location, we see no clear correlation between the magnitudes or directions of the ionospheric magnetic field and the surface magnetic field as might be expected. If the presumed ionospheric currents have a small scale size, then the ionospheric magnetic field will display increased variability as MAVEN flies through the current structure. Whereas the present analysis is restricted to mostly nightside MAVEN overflights where current are expected to be weak, future analyses should incorporate dayside overflights where current are expected to be stronger and current signatures more clear.

1 **A first comparison between ionospheric and surface level magnetic fields at Mars**

2 **M. O. Fillingim[1], C. L. Johnson[2,3], A Mittelholz[2], B. Langlais[4], C. T. Russell[5], S. Joy[5], P.**
3 **Chi[5], R. J. Lillis[1], J. Espley[6], S. Smrekar[7], W. B. Banerdt[7], and B. M. Jakosky[8]**

4 [1]Space Sciences Laboratory, University of California, Berkeley, CA, USA.

5 [2]Department of Earth, Ocean and Atmospheric Sciences, University of British Columbia,
6 Vancouver, BC, Canada.

7 [3]Planetary Science Institute, Tucson, AZ, USA.

8 [4]Laboratoire de Planétologie et Géodynamique, UMR CNRS 6112, Université de Nantes,
9 France.

10 [5]Department of Earth, Planetary and Space Sciences, University of California, Los Angeles, CA,
11 USA.

12 [6]Planetary Magnetospheres Laboratory, NASA Goddard Space Flight Center, Greenbelt, MD,
13 USA.

14 [7]Jet Propulsion Laboratory, California Institute of Technology, Pasadena, CA, USA.

15 [8]Laboratory for Atmospheric and Space Physics, University of Colorado Boulder, CO, USA.

16 Corresponding author: Matthew Fillingim (matt@ssl.berkeley.edu)

17 **Key Points:**

18 • Ionospheric magnetic fields are compared to surface magnetic fields at Mars for the first
19 time

20 • The direction of the surface crustal field is detectable up to 250 km altitude

21 • Variations in the residual fields are suggestive of weak but highly variable ionospheric
22 currents
23

24 **Abstract**

25 With both the Mars Atmosphere and Volatile Evolution (MAVEN) mission and the Interior
26 Exploration using Seismic Investigations, Geodesy and Heat Transport (InSight) mission
27 concurrently operating at Mars, we are able to make two point comparisons of the vector
28 magnetic field at Mars for the first time. During MAVEN overflights of the InSight landing site,
29 we compared deviations in the ionospheric magnetic field to variations in the surface level
30 magnetic field. We find significant orbit to orbit variability in the magnitude and direction of the
31 ionospheric magnetic field as well as significant day to day variability of the surface level
32 magnetic field. We attribute this variability to time varying ionospheric currents. However, when
33 analyzing the ensemble of 16 individual MAVEN overflights of the InSight landing location, we
34 see no clear correlation between the magnitudes or directions of the ionospheric magnetic field
35 and the surface magnetic field as might be expected. If the presumed ionospheric currents have a
36 small scale size, then the ionospheric magnetic field will display increased variability as
37 MAVEN flies through the current structure. Whereas the present analysis is restricted to mostly
38 nightside MAVEN overflights where current are expected to be weak, future analyses should
39 incorporate dayside overflights where current are expected to be stronger and current signatures
40 more clear.

41 **Plain Language Summary**

42 Two mission currently operating at Mars have instruments that measure magnetic fields: the
43 Mars Atmosphere and Volatile Evolution (MAVEN) mission which has been orbiting Mars since
44 September 2014 and the Interior Exploration using Seismic Investigations, Geodesy and Heat
45 Transport (InSight) mission which landed on the surface of Mars in November 2018. This allows
46 us to make two point comparisons of the magnetic field at Mars for the first time. We compare
47 the magnetic field in the upper atmosphere below 250 km altitude measured by MAVEN to the
48 magnetic field at the surface measured by InSight during times when MAVEN is directly above
49 InSight. The magnetic field measured by MAVEN shows considerable variability from orbit to
50 orbit over the same location. At the same time, the surface magnetic field measured by InSight
51 shows considerable day to day variations. We suggest that this variability is caused by electric
52 currents flowing in the upper atmosphere of Mars in the vicinity of MAVEN.

53 **1 Introduction**

54   For well over a century, surface level magnetic field measurements have been used to
55 study atmospheric, ionospheric, and magnetospheric dynamics at Earth (e.g., Schuster, 1889;
56 Birkeland, 1908) Spatial and temporal changes in current systems and magnetic field
57 configurations can be inferred remotely from changes in the magnetic fields they produce. With
58 the landing of InSight on Mars in the near equatorial Elysium Planitia on 26 November 2018, the
59 InSight FluxGate magnetometer (IFG) now provides the first surface level magnetic field
60 measurements on another planet (Banfield et al., 2018). Already, time variations in the measured
61 magnetic field have been interpreted as resulting from atmospheric/ionospheric and
62 magnetospheric processes (Johnson et al., 2020; Mittelholz et al., 2020).

63   Additionally, the Mars Atmosphere and Volatile Evolution Mission, MAVEN, has been
64 orbiting Mars since September 2014 (Jakosky et al., 2015). MAVEN carries a suite of plasma
65 instruments, including the only currently operating magnetometer in orbit (Connerney et al.
66 2015), in order to characterize the upper atmosphere and space environment around Mars

67 including the solar wind, magnetosheath, magnetotail, and ionosphere. Its elliptical orbit
68 typically brings MAVEN to within ~ 150 km of the surface, directly sampling the neutral and
69 plasma constituents (Mahaffy et al., 2014, McFadden et al., 2015) as well as the ambient
70 magnetic field (Connerney et al., 2015) in the upper atmosphere.

71 Thus, starting with InSight operations in late 2018, two-point vector magnetic field
72 measurements are possible at Mars for the first time. We are able to compare changes in the
73 magnetic field in the ionosphere to changes in the surface magnetic field in order to determine
74 the sources of the variability in the surface magnetic field. Here, we focus on intervals when
75 MAVEN was in the ionosphere directly overhead InSight.

76 Magnetic field perturbations due to changing ionospheric currents can be measured on
77 the ground. Recently, Lillis et al. (2019) computed the expected magnetic field perturbations due
78 to neutral wind driven currents in the ionosphere. They predicted surface level magnetic field
79 variations of a few tens of nT. Johnson et al. (2020) interpreted the repeatable diurnal variation in
80 the surface level magnetic field measured by IFG as a result of ionospheric currents.
81 Additionally, Mittelholz et al. (2020), by looking at over one Earth year of IFG data, reported
82 evidence of seasonal changes in the diurnal magnetic field signal consistent with seasonal
83 changes in the modeled thermospheric winds which drive ionospheric currents.

84 Here, we compare in-situ MAVEN magnetic field measurements in the ionosphere above
85 InSight to IFG surface level magnetic field measurements in an attempt to correlate changes in
86 the surface magnetic field to ionospheric dynamics. In the next section, we summarize the data
87 and data selection criteria. In Section 3, we compare MAVEN and IFG data from different
88 individual MAVEN overflights at the same local time and statistically compare the variations in
89 the surface magnetic field to deviations in the ionosphere magnetic field. Finally we discuss the
90 result and future directions.

91 **2 Data and Data Selection**

92 On 26 November 2018 InSight landed on Mars at 4.50^o N, 135.63^o E in Elysium Planitia
93 (Banerdt et al., 2020). As part of the Auxiliary Payload Sensor Suite (APSS), InSight carries a
94 fluxgate magnetometer with the primary purpose of measuring the magnetic field environment to
95 characterize and remove this from the seismic data (Banfield et al., 2018). The sampling rate of
96 the IFG is 20 Hz which is decimated to 0.2 Hz or 2 Hz depending upon telemetry constraints.
97 Limited 20 Hz data can additionally be downlinked on request from the science team [Johnson et
98 al., 2020]. In this study we use the decimated data (either 0.2 or 2 Hz) in the Lander Level Frame
99 in which X is North, Y is East and, Z is vertically Down (i.e., NED coordinates) [Joy et al.,
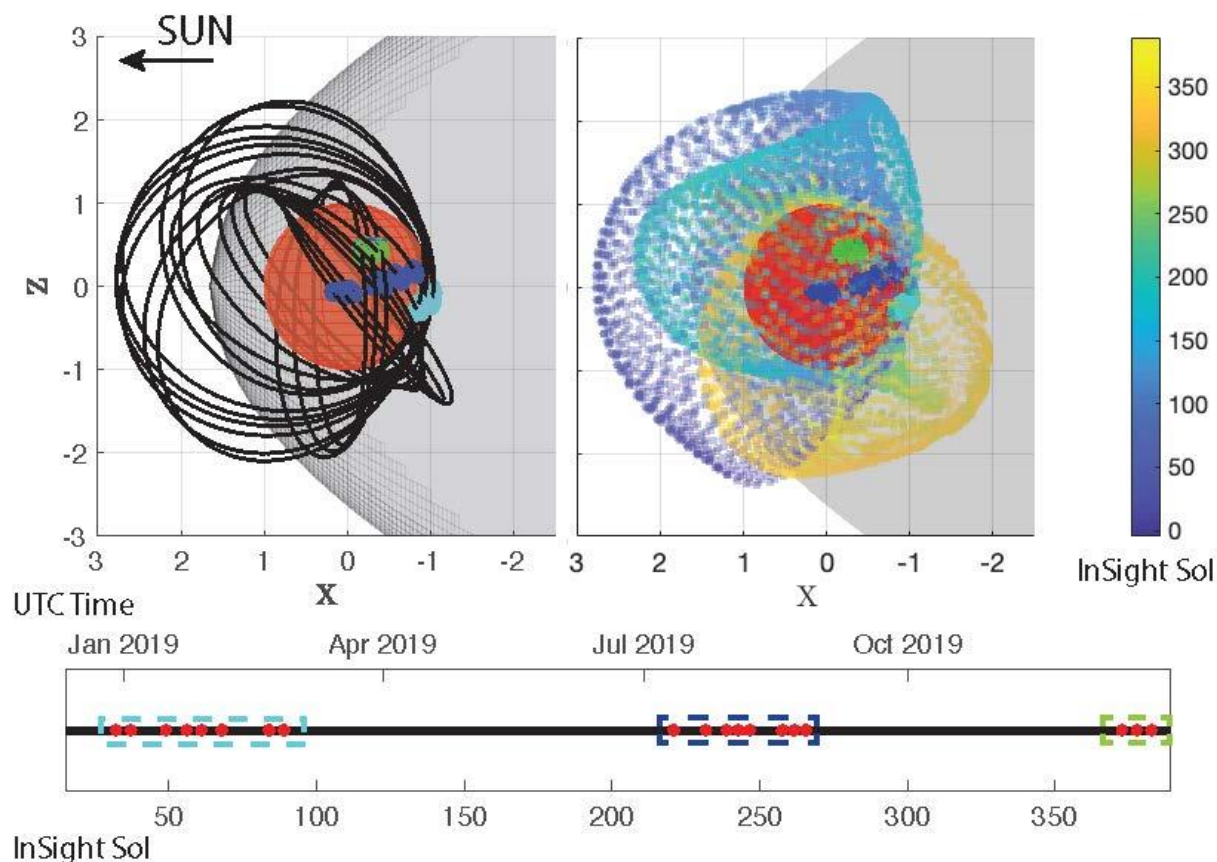100 2019].

101 The MAVEN magnetometer (MAG) (Connerney et al., 2015) has been observing the
102 magnetic environment around Mars since orbit insertion in September 2014. The intrinsic
103 sampling rate is 32 Hz. In this study we use the 1-second averaged data products as provided on
104 the Planetary Data System (PDS).

105 It is well known that some regions of the martian crust are magnetized resulting in crustal
106 magnetic fields (Acuna et al., 2001). InSight is in a region of moderate magnetization between
107 the weakly magnetized northern hemisphere and the more strongly magnetized southern
108 hemisphere (Mittelholz et al., 2018; Johnson et al., 2020). In order to determine the magnetic
109 field variations due to ionospheric electric currents, we must remove the crustal contribution

110 from the MAVEN-measured magnetic field. For this, we use the recent global magnetic field
111 model of Langlais et al. (2019) (hereafter referred to as L19).This is the first global model to
112 incorporate lower altitude MAVEN data down to 150 km. The spatial resolution of the model is
113 ~ 160 km which corresponds to a spherical harmonic model degree of 134.

114   During January/February 2019, July/August 2019, and December 2019/January 2020,
115 MAVEN's periapsis (at ~150 km altitude) was above the InSight landing site. Here we focus on
116 the first two of these time intervals, January/February 2019 and July/August 2019, as both
117 MAVEN and IFG data are available from the PDS for these intervals. As of this writing, the data
118 covering the complete third interval were not available. For our analysis, we selected intervals
119 when MAVEN was within +/- 4° latitude and longitude of InSight and at altitudes less than 250
120 km Figure 1 graphically shows the MAVEN orbit during these intervals and the location of
121 InSight in local time during the MAVEN overflights.

122   Table 1 lists the time intervals when these criteria were satisfied as well as the mean local

Figure 1: An overview of MAVEN coverage for InSight sols 1-389. The left panel only shows orbits that passed within a 4 degree circle of InSight Landing Site and below 250 km. The track sections discussed in this paper are highlighted in color according to sampling time in January/February (cyan), July/August (blue) and December (green) (January 2020 data were not yet publicly available). The right panels show every 5000th MAVEN data point (from the 1 Hz data) for every orbit during this time frame color coded according to InSight sol. The grey area represents a model bow shock (Vignes et al., 2000). The bottom timeline highlights areas at which overflights occurred using the same coloring scheme as above.
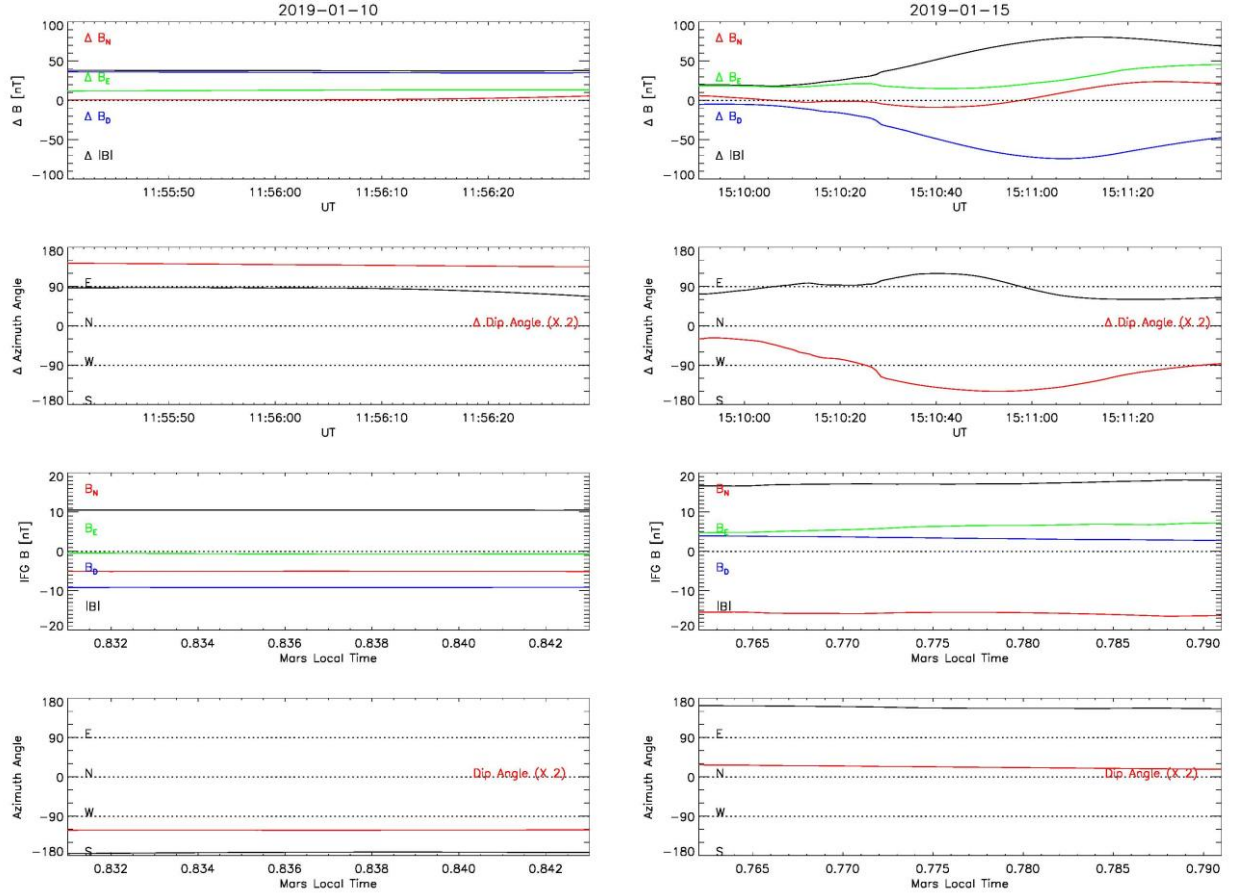
123   solar time at the InSight landing site. Of the twenty MAVEN overflight intervals, a total of
124   sixteen intervals of coincident MAVEN and IFG data were analyzed. As noted in Table 1, no
125   IFG data were available for three MAVEN overflights; these data gaps were due to Payload
126   Auxiliary Electronics (PAE) anomalies on the InSight lander. A further interval (on 15 July
127   2019) was excluded from analysis due to the short duration of the overflight (< 10 seconds)
128   because the MAVEN trajectory just skimmed the edge of the +/- 4° region around InSight. Most
129   overflights last one to two minutes as MAVEN traverses a larger span of the region (up to ~ 500
130   km) traveling at speed of a few km per second.

131

Start time (UT)	End time (UT)	MLST
2018-12-29/05:09:20	2018-12-29/05:10:00	no IFG data
2019-01-03/08:20:00	2019-01-03/08:21:20	01:51
2019-01-10/11:55:40	2019-01-10/11:56:30	00:50
2019-01-15/15:09:50	2019-01-15/15:11:40	00:47
2019-01-22/18:52:20	2019-01-22/18:53:20	23:52
2019-01-27/22:10:10	2019-01-27/22:12:00	23:53
2019-02-04/01:53:50	2019-02-04/01:55:40	23:02
2019-02-09/05:16:40	2019-02-09/05:17:00	23:06
2019-02-20/11:18:10	2019-02-20/11:20:10	21:56
2019-02-25/14:17:50	2019-02-25/14:19:50	21:40
2019-07-11/04:42:00	2019-07-11/04:43:40	21:42
2019-07-15/07:21:20	2019-07-15/07;21:20	duration < 10 sec
2019-07-18/08:22:20	2019-07-18/08:22:30	20:48
2019-07-22/10:58:50	2019-07-22/11:00:40	no IFG data
2019-07-29/14:35:50	2019-07-29/14:36:30	19:52
2019-08-02/17:10:10	2019-08-02/17:12:00	19:49
2019-08-06/19:39:40	2019-08-06/19:40:30	no IFG data
2019-08-18/01:18:50	2019-08-18/01:20:30	18:11
2019-08-22/03:38:40	2019-08-22/03:40:20	17:53
2019-08-26/05:57:50	2019-08-26/05:58:10	17:35

132   **Table 1:** Start and end times of MAVEN overlights for the periods highlighted in cyan and blue
133   in Figure 1. The third column lists the Mean Local Solar Time at the InSight landing site
134   whenever IFG data is available. No IFG data was collected during Payload Auxiliary Electronics
135   anomalies.

136

137   As can be seen in Figure 1 and Table 1, most of the overflights occurred during
138   nighttime, in the dusk and midnight local time sectors, due to the orbit geometry of MAVEN. As
139   mentioned below, this fact complicates the interpretation since ionospheric current densities are
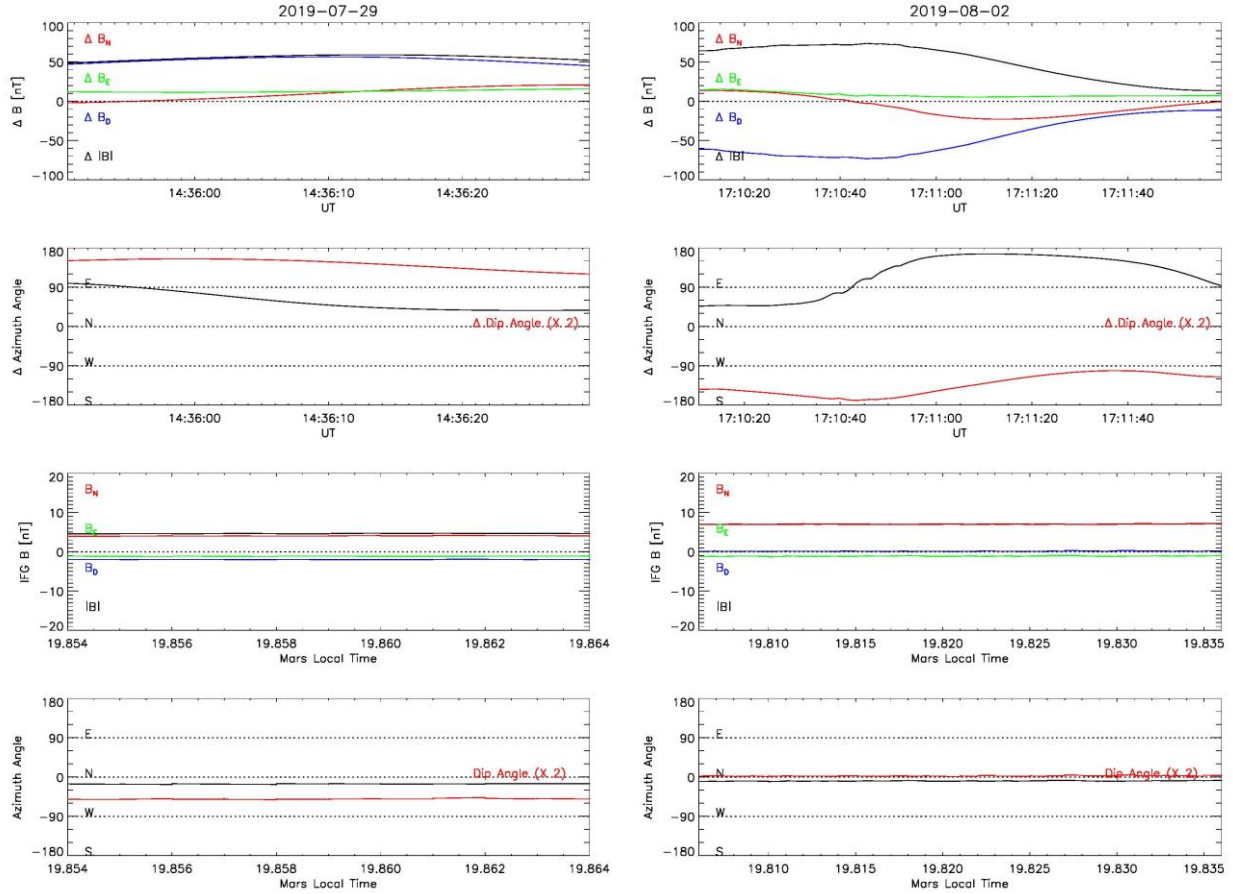140   expected to be much lower at night due to the smaller plasma density.

141 **3 Results**

Figure 2: Examples of magnetic field data on two orbits from the 10 January 2019, InSight sol 44 (left) and 15 January 2019, sol 49 (right) overflights of InSight by MAVEN. In each column, the top panel shows the residual ionospheric magnetic field in North, East, Down components (in red, green, blue, respectively) as well as the magnitude of the residual magnetic field. The second panel shows the azimuth angle (black) and dip angle (multiplied by a factor of 2, red) of residual ionospheric magnetic field. The third panel shows the residual surface magnetic field in the same coordinate system as the top panel. The bottom panel shows the corresponding azimuth and dip angles for the residual surface magnetic field. The ionospheric data are plotted against Universal Time while the surface data are plotted against Mars Mean Solar Local Time.

142   Figures 2 and 3 show examples of ionospheric magnetic field data from MAVEN and
143 surface magnetic field data from IFG for two different overflights that occurred at approximately
144 the same local time. Figure 2 compares data from 10 January 2019 (InSight sol 44) and 15
145 January 2019 (sol 49) collected just past midnight Mars local time (~ 00:50 local time). Figure 3
146 compares data from 29 July 2019 (sol 238) and 2 August 2019 (sol 242). In all cases, the top
147 panel shows the residual ionospheric magnetic field - i.e., the ionospheric magnetic field
148 measured by MAVEN with the L19 magnetic field model subtracted - in NED coordinates. The
149 second panel shows the azimuth and dip angles of the residual ionospheric field. The azimuth
150 angle is measured clockwise from north, and the dip (or inclination) angle is measured positive
151 downward from horizontal. In the second (and fourth panels), the dip angle is multiplied by a
152 factor of 2 for clarity. The third panel shows the residual surface magnetic field measured by IFG
153 in NED coordinates. The median of each component was computed for each 60-day overflight

Figure 3: Same as Figure 2 except for 29 July 2019, sol 238 (left) and 2 August 2019, sol 242 (right).

154 interval (January/February 2019 and July/August 2019 separately) and subtracted from the IFG
155 measured surface field. Finally, the fourth panel shows the azimuth and dip angles of the residual
156 surface magnetic field.

157   It can be seen in both Figures that even though MAVEN is passing over the same region
158 Mars, the residual ionospheric magnetic field varies from orbit to orbit. For example, on 10
159 January 2019, the residual magnetic field is small (< 15 nT) and relatively stable in direction.
160 Five days later, when MAVEN traverses nearly the same trajectory, there are significant
161 variations in the residual ionospheric magnetic field, particularly in the vertical (D) component;
162 the azimuthal component rotates by nearly 90° and the dip angle changes sign. Likewise, there
163 are day to day differences in the surface magnetic field even at the same local time. From 10
164 January to 15 January 2019, the magnitude of the residual surface magnetic field also increases
165 by nearly 10 nT, and the dip angle changes from negative to positive (upward pointing to
166 downward pointing). Similar, though not quite as extreme variations are seen when comparing
167 29 July and 2 August 2019 in Figure 3.

168   Even though the possibility of small scale magnetic fields of crustal origin that are not
169 captured by the model cannot be completely ruled out, we interpret this orbit to orbit variability
170 in the ionospheric field as resulting from variability in small scale ionospheric current structures.
171 The steep slope in the residual magnetic field near 15:10:27 UT on 15 January 2019, particularly
172 in the vertical component and the dip angle, is consistent with the magnetic signature of a thin
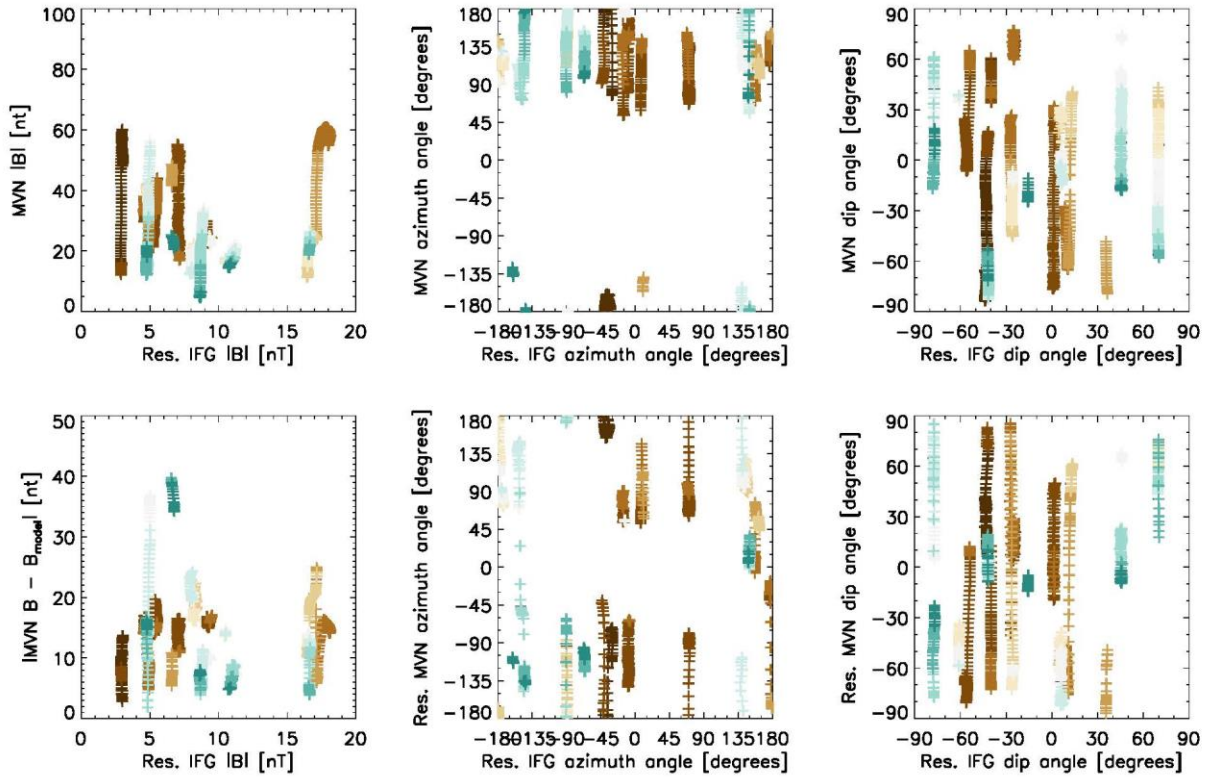
173 current layer. Similarly, the more gradual change in sign of the vertical component and dip angle
174 would be consistent with a broader current. From a single observation platform, it is impossible
175 to uniquely determine the geometry of a current system that would produce similar magnetic
176 deflections, so we refrain from speculating too much about the direction of such a current
177 system.

178   Changes in the residual surface field magnitude and direction would also result from
179 time-varying ionospheric currents. From 10 January to 15 January, the vertical component of the
180 residual surface field changes from negative to slightly positive (upward pointing to nearly
181 horizontal) and the north component increases in magnitude (becomes more southward) by ~ 10
182 nT. Assuming the current is above InSight (a reasonable assumption in this case), this would be
183 consistent with the appearance or intensification of a westward current in the ionosphere above
184 the lander. However, again, we caution that it is ill-advised to try to extrapolate too much about
185 the current configurations given limited observation points.

186   For a more statistical view, Figure 4 compares the ionospheric magnetic field to the
187 residual surface magnetic field for all 16 intervals. The first column shows a scatter plot of the
188 magnitude of the total ionospheric magnetic field as measured by MAVEN when it is over
189 InSight and the magnitude of the residual surface magnetic field from IFG. The second column
190 shows the azimuth angle of the ionospheric magnetic field versus the azimuth angle of the
191 residual surface magnetic field. The third column plots the dip angle of the ionospheric field
192 versus the dip angle of the surface magnetic field. The bottom row plots the same quantities
193 except the vertical axes represent the residual ionospheric field: the observed magnetic field
194 minus the model crustal magnetic field of L19 (i.e., the same data as shown in Figures 2 and 3).
195 The color in all panels corresponds to altitude. Brown shades represent ionospheric data below
196 200 km while blue shades represent data above 200 km. The tint increases (becomes whiter) near
197 200 km and the shade increases (becomes darker) toward the extremes of 150 km and 250 km.
198 Since the MAVEN data typically vary more than the IFG data during each individual, the
199 vertical stripes on the plots can be interpreted as individual overflights of MAVEN.

200   Several things are immediately noticeable from this comparison. In general, the
201 magnitude of the ionosphere magnetic field is slightly larger at lower altitudes (top row, left
202 panel). This is expected since InSight is located in a region of moderate crustal magnetic field.
203 The azimuth angle of the total ionospheric magnetic field is generally in the south-east direction,
204 between 90 and 180 degrees (top row, middle panel). This is in general agreement with the
205 direction of the total (not residual) surface magnetic field. As reported in Johnson et al. (2020),
206 the azimuth angle of the average total surface magnetic field is 139° suggesting that the influence
207 of the surface magnetic field reaches to at least 250 km altitude. The dip angle of the ionospheric
208 magnetic field does not appear to have any correlation with altitude or the surface magnetic field.
209 The dip angle of the average total surface field is -27° (Johnson et al., 2020). The ionospheric
210 magnetic field dip angle varies substantially at all altitudes.

211   From the top row of Figure 4, it is clear that there is substantial variation in the
212 magnitude, azimuth angle and dip angle of the residual surface magnetic field. However, there
213 does not appear to be any clear correlation between the total ionospheric magnetic field and the
214 residual surface magnetic field.

Figure 4: Top row, left to right: total ionospheric magnetic field strength, |B|, as measured by MAVEN above InSight versus the magnitude of the residual (demeaned) surface magnetic field from IFG, ionospheric magnetic field azimuthal angle versus the surface magnetic field azimuthal angle, ionospheric magnetic field dip angle versus the surface magnetic field dip angle. Bottom row: same quantities except with the crustal magnetic field prediction of Langlais et al. (2019) removed from the ionospheric magnetic field. Colors represent altitude. Brown colors correspond to ionospheric altitudes below 200 km, and blue colors correspond to altitudes above 200 km.

215 The magnitude of the residual ionospheric magnetic field (bottom row, left panel) is
216 generally much lower than the magnitude of the total ionospheric magnetic field (note the change
217 in the vertical axis between the top left and bottom left panels in Figure 4), suggesting that the
218 crustal magnetic field model of L19 does take into account a significant part of the crustal
219 magnetic field contribution. Additionally, the largest residual ionosphere magnetic fields occur at
220 the highest altitudes analyzed. In fact, residual ionospheric magnetic field magnitudes greater
221 than 25 nT only occur at altitudes higher than 200 km. We should note that the largest residual
222 ionospheric magnetic fields also occur at the earliest local times – those MAVEN overflights at
223 or just before dusk when the ionosphere is still sunlit. However, there does not appear to be a
224 correlation between the magnitude of the residual ionospheric magnetic field and the magnitude
225 of the residual surface field. When only considering the lowest altitude ionospheric data (dark
226 brown points), there may be a weak correlation between the magnitude of the residual
227 ionospheric magnetic field and the magnitude of the residual surface magnetic field, but there
228 are too few data points to make a clear determination.

229   If the variations in the surface magnetic field are presumed to be due to ionospheric
230 currents, one may expect a relationship between the azimuth angle of the residual ionospheric
231 magnetic field and the azimuth angle of the residual surface magnetic field. If, for example,
232 ionospheric currents with peak current densities near 150 km (Fillingim et al., 2012; Lillis et al.,
233 2019) cause a deviation in the azimuth angle at the surface, one would expect the deviation in the
234 azimuth angle in the ionospheric magnetic field above the current to be different from the surface
235 deviation by 180°. A westward current would cause a southward deviation in the surface
236 magnetic field and a northward deviation in the ionospheric magnetic field above the current. No
237 such relationship is seen in Figure 4 (bottom row, middle panel); the azimuth angles of the
238 residual ionospheric magnetic field and the surface magnetic field appear uncorrelated.

239   Additionally, there does not appear to be a clear correlation between the residual
240 ionospheric magnetic field dip angle and the residual surface dip angle (bottom row, right panel).
241 In general, for a given residual dip angle in the surface field, there is an extremely broad range of
242 residual dip angles in the ionosphere - in some cases spanning nearly 180 degrees. This lack of
243 correlation may in part be explained by MAVEN traveling through small scale ionospheric
244 current structures where the residual magnetic field direction may vary significantly over several
245 degrees of latitude (such as seen in the right columns of Figures 2 and 3).

4 Conclusions

247   With MAVEN and InSight data, we are able to make two-point vector magnetic field
248 comparisons in the ionosphere and on the surface of Mars for the first time. These comparisons
249 can reveal the sources of magnetic field variability on the surface of Mars, and at the same time
250 may lead to new insights into atmospheric, ionospheric, and magnetospheric dynamics.

251   From analyzing individual MAVEN overflights of the InSight landing site, we note
252 significant orbit to orbit variation in the ionospheric magnetic field coincident with day to day
253 variations in the surface magnetic field even at nearly identical local times. One interpretation is
254 that time varying ionospheric currents, which would cause orbit to orbit variations in the
255 ionospheric magnetic field, may be the cause of day to day magnetic field variations on the
256 surface.

257   Ionospheric current variability can be driven by internal (neutral winds) or external (solar
258 wind and interplanetary magnetic field) sources. Recent measurements of thermospheric neutral
259 winds by MAVEN have shown that neutral winds can exhibit significant orbit to orbit variations
260 as well as substantial deviation from global circulation model predictions (Roeten et al., 2019).
261 Additionally, changing interplanetary magnetic field conditions can affect the magnetic field at
262 ionospheric altitudes, even on the nightside (e.g., Brain et al., 2003), which can in turn impact
263 the strength and direction of ionospheric currents.

264   The lack of correlation between ionospheric and surface magnetic field deviations may
265 argue against ionospheric currents as being the source of the orbit to orbit and day to day
266 variations in the magnetic field deviations. However, small scale currents (<< 100 km), which
267 will produce a given magnetic field signature at a fixed location on the surface, may be observed
268 as a relatively broad range of magnetic field magnitudes and directions as a spacecraft traverses
269 the current producing region. We could attempt to restrict ionospheric data to within say +/- 1°
270 (+/- ~ 60 km) of the InSight location to remove some degree of variability caused by spacecraft

271 motion; however, the number of overflights would decrease to a statistically insignificant
272 number.

273   Another complicating factor in the above analysis and interpretation is that the available
274 data thus far is primarily on the nightside. Nighttime ionosphere currents are expected to be weak
275 due to the low plasma density (e.g., Lillis et al., 2019). Weak currents will produce smaller
276 magnetic field deviations at the surface. Stronger ionospheric currents on the dayside may
277 provide a more clear signal in the surface and ionospheric magnetic field deflections. As
278 MAVEN's orbit continues to precess in the InSight era, future overflight opportunities (which
279 occur with an approximate cadence of six months) will occur on the dayside.

291 **References**

292 Acuña, M. H., J. E. P. Connerney, P. Wasilewski, R. P. Lin, D. Mitchell, K. A. Anderson, et al.
293   (2001), Magnetic field of Mars: Summary of results from the aerobraking and mapping
294   orbits, *J. Geophys. Res.*, 106(E10), 23403-23417, doi:10.1029/2000JE001404.

295 Banfield, D., J. A. Rodriguez-Manfredi, C. T. Russell, K. M. Rowe, D. Leneman, H. R. Lai, et
296   al. (2018), InSight Auxiliary Payload Sensor Suite (APSS), Space Sci. Rev., 215, 4,
297   doi:10.1007/s11214-018-0570-x.

298 Banerdt, W. B., S. E. Smrekar, D. Banfield, D. Giardini, M. Golombek, C. L. Johnson, et al.
299   (2020), Initial results from the InSight mission on Mars, *Nat. Geosci.*, 13, 183-189,
300   doi:10.1038.s41561-020-0544-y.

301 Birkeland, K. (1908), *The Norwegian Aurora Polaris Expedition 1902-1903*, Vol. 1, H.
302   Aschehoug & Co., Christiania (Oslo)
303   (https://archive.org/details/norwegianaurorap01chrrich).

304 Brain, D. A., Bagenal, F., Acuña, M. H., and Connerney, J. E. P. (2003), Martian magnetic
305   morphology: Contributions from the solar wind and crust, *J. Geophys. Res.*, 108(A12),
306   1424, doi:10.1029/2002JA009482.

307 Connerney, J. E. P., Espley, J., Lawton, P., Murphy, S., Odom, J., Oliversen, R., & Sheppard, D.
308   (2015), The MAVEN Magnetic Field Investigation, *Space Sci. Rev.*, 195, 257-291,
309   doi:10.1007/s11214-015-0169-4.

310 Fillingim, M. O., Lillis, R. J., England, S. L., Peticolas, L. M., Brain, D. A., Halekas, J. S., et al.
311   (2012), On wind-driven electrojets at magnetic cusps in the nightside ionosphere of Mars,
312   *Earth Planet Space*, 64, 5, doi:10.5047/eps.2011.04.010.

313 Jakosky, B. M., Grebowsky, J. M., Luhmann, J. G., & Brain, D. A. (2015), Initial results from
314   the MAVEN mission to Mars, *Geophys. Res. Lett.*, 42, 8791–8802,
315   doi:10.1002/2015GL065271.

316 Johnson, C. L., Mittelholz, A., Langlais, B., Russell, C. T., Ansan, V., Banfield, D., et al. (2020),
317   Crustal and time-varying magnetic fields at the InSight landing site on Mars, *Nat.
318   Geosci.*, 13, 199-204, doi:10.1038/s41561-020-0537-x.

319 Joy, S. P., Mafi, J. N., & Slavney, S. (2019), Interior Exploration Using Seismic Investigations,
320   Geodesy, and Heat Transport (InSight) Mission Insight Fluxgate Magnetometer (IFG)
321   PDS Archive Software Interface Specification, *urn:nasa:pds:insight-ifg-
322   mars:document:insight-ifg-sis*.

323 Langlais, B., Thébault, E., Houliez, A., Purucker, M. E., & Lillis, R. J. (2019), A new model of
324   the crustal magnetic field of Mars using MGS and MAVEN, *J. Geophys. Res. Planets*,
325   124, 1542–1569, doi:10.1029/2018JE005854.

326 Lillis, R. J., Fillingim, M. O., Ma, Y., Gonzalez-Galindo, F., Forget, F., Johnson, C. L., et al.
327   (2019), Modeling wind-driven ionospheric dynamo currents at Mars: Expectations for
328   InSight magnetic field measurements, *Geophys. Res. Lett.*, 46, 5083– 5091,
329   doi:10.1029/2019GL082536.

330 Mahaffy, P. R., Benna, M., King, T., Harpold, D. N., Arvey, R., Barciniak, M., et al. (2014), The
331   Neutral Gas and Ion Mass Spectrometer on the Mars Atmosphere and Volatile Evolution
332   Mission, *Space Sci. Rev.*, 195, 49-73, doi:10.1007/s11214-014-0091-1.

333 McFadden, J. P., Kortmann, O., Curtis, D., Dalton, G., Johnson, G., Abiad, R., et al. (2015),
334   MAVEN SupraThermal and Thermal Ion Compostion (STATIC) Instrument, *Space Sci.
335   Rev.*, 195, 199-256, doi:10.1007/s11214-015-0175-6.

336 Mittelholz, A., Johnson, C. L., & Morschhauser, A. (2018), A new magnetic field activity proxy
337   for Mars from MAVEN data, *Geophys. Res. Lett.*, 45, 5899– 5907,
338   doi:10.1029/2018GL078425.

339 Mittelholz, A., Johnson, C. L., Thorne, S. N., Joy, S., Barrett, E., Clinton, J., et al. (2020), The
340   origin of observed magnetic variability for a sol on Mars from InSight, *J. Geophys. Res.
341   Planets*, submitted. (*I know papers submitted or in press are not allowed, but this
342   manuscript was submitted as part of the same special collection*)

343 Roeten, K. J., Bougher, S. W., Benna, M., Mahaffy, P. R., Lee, Y., Pawlowski, D., et al. (2019),
344   MAVEN/NGIMS thermospheric neutral wind observations: Interpretation using the M-
345   GITM general circulation model, *J. Geophys. Res. Planets*, 124, 3283– 3303,
346   doi:10.1029/2019JE005957.

347 Schuster, A. (1889), The diurnal variation of terrestrial magnetism, *Philos. Trans. R. Soc. A*, 180,
348   467-518, doi:10.1098.rsta.1889.0015.

349 Vignes, D., Mazelle, C., Rème, H., Acuña, M. H., Connerney, J. E. P., Lin, R. P., et al. (2000),
350   The solar wind interaction with Mars: Locations and shapes of the bow shock and the

351   magnetic pile-up boundary from the observations of the MAG/ER Experiment onboard
352   Mars Global Surveyor, Geophys. Res. Lett., 27, 49-52, doi:10.1029/1999GL010703.